frontiers | Frontiers in Physics

TYPE Original Research
PUBLISHED 19 January 2026
DOI 10.3389/fphy.2026.1732730

OPEN ACCESS

EDITED BY
Rajib Biswas,
Tezpur University, India

REVIEWED BY
Shubhranil Maity,
Asst. Manager, R&D, India
Javier Antonio Martin Vela,
Instituto Tecnológico de Mérida, Mexico

*CORRESPONDENCE
Imran Aziz,
imran.aziz@physics.uu.se
Ahmad Almogren,
ahalmogren@ksu.edu.sa

†PRESENT ADDRESS
Jawad Mirza,
SEECS Photonics Research Group,
Islamabad, Pakistan

RECEIVED 26 October 2025
REVISED 15 December 2025
ACCEPTED 02 January 2026
PUBLISHED 19 January 2026

CITATION
Mirza J, Atieh A, Boynukalın S, Kanwal B, Aziz I and Almogren A (2026) Design of 12.5 MHz ultrashort passively mode-locked Figure-9 holmium-doped fiber laser implemented using different reflectors.
Front. Phys. 14:1732730.
doi: 10.3389/fphy.2026.1732730

Design of 12.5 MHz ultrashort passively mode-locked Figure-9 holmium-doped fiber laser implemented using different reflectors

Jawad Mirza[1†], Ahmad Atieh[2], Serhat Boynukalın[3], Benish Kanwal[4], Imran Aziz[4,5]* and Ahmad Almogren[6]*

[1]Electrical Engineering Department, HITEC University Taxila, Taxila, Pakistan, [2]Optiwave Systems Inc., Ottawa, ON, Canada, [3]Department of Railway Systems Engineering, Istanbul Technical University, Istanbul, Türkiye, [4]Electrical Engineering Department, Mirpur University of Science and Technology, Mirpur (AJK), Pakistan, [5]Department of Physics and Astronomy, Uppsala University, Uppsala, Sweden, [6]Department of Computer Science, College of Computer and Information Sciences, King Saud University, Riyadh, Saudi Arabia

Special cavities like Figure-8 and Figure-9 are exploited in lasers to enable self-starting passive mode-locking using nonlinear amplifying loop mirrors (NALMs) or nonlinear optical loop mirrors (NOLMs). Their significance lies in enhanced nonlinearity and intracavity feedback, enabling stable, self-sustained mode-locked pulses suitable for ultrafast fiber lasers. In this paper, we propose the design of femtosecond pulse width passively mode-locked Holmium-doped fiber laser (HDFL) operating at 2090 nm and 12.5 MHz repetition rate based on Figure-9 (F9) cavity. The F9 cavity is implemented utilizing three different reflectors, including saturable absorber (SA), simple mirror (SM), and fiber loop mirror (FLM). The performance of the proposed laser is compared for different reflectors considering characteristics of slope efficiency (SE), pulse width, optical signal to noise ratio (OSNR), peak power, and pulse energy. SA, SM, and FLM configurations yield mode-locked pulses with SEs of 35.6%, 8%, and 8.8%, pulse widths of 357.2 fs, 294 fs, and 231 fs, OSNRs of 36.4 dB, 46 dB, and 50 dB, peak powers of 13.53 kW, 6.12 kW, and 9 kW, and pulse energies of 4.83 nJ, 2 nJ, and 2.1 nJ, respectively. The analysis reveals that the FLM-based reflector achieves the shortest pulse width and highest OSNR, while the SA-based reflector delivers the highest peak power and pulse energy, highlighting trade-offs between pulse quality and energy performance in the proposed laser design.

KEYWORDS

fiber loop mirror, figure-9 cavity, holmium-doped fiber laser, nonlinear amplifying loopmirror, passive mode-locking, pulse energy, saturable absorber, slope efficiency

1 Introduction

An ultrashort pulsed laser has an extremely short pulse width and high peak power and is used for a variety of specialized applications [1]. For example, ultrashort high peak power mode-locked HDFLs operating around 2100 nm eye-safe optical window have got significant research interest due to their applications in different

important areas such as remote sensing, LiDAR, deep space optical communications, and surgical procedures due to reduced light scattering in human tissues and atmospheric absorption [1,2]. The primary active fibers for 2100 nm applications include Thulium-doped fibers (TDFs), Thulium-Holmium co-doped fibers (THDFs), and Holmium-doped fibers (HDFs) [3]. Notably, HDFs offer superior gain performance compared to TDFs and THDFs at wavelengths exceeding 2100 nm [4].

Mode-locked HDFLs can be implemented through either passive or active techniques [5]. Passive mode-locking employs a SA within the laser cavity, whereas active mode-locking utilizes an external modulator, such as Mach-Zehnder modulator (MZM) driven by a pulse generator to create periodic loss modulation [5]. Among these approaches, passively mode-locking offers distinct advantages for generating ultrashort pulses entirely in optical domain, including simpler cavity design, higher SE, higher peak power and easier implementation compared to active techniques [6]. Due to these advantages, numerous mode-locking mechanisms have been explored in HDFLs, including semiconductor saturable absorber mirrors (SESAMs), carbon nanotubes, graphene, and black phosphorus [3]. However, recent research has increasingly focused on specialized cavity designs, such as F8 and F9 configurations, which leverage NOLMs and NALMs for robust, self-starting mode-locking [3]. These configurations offer superior performance in terms of pulse stability, environmental insensitivity, and power scalability compared to above mentioned approaches. The F9 cavity, in particular, has gained significant attention due to its simpler architecture and enhanced nonlinearity control, making it ideal for high-repetition-rate, ultrashort-pulse generation in the 2100 nm spectral region [7].

The F9 laser cavities have been extensively investigated utilizing different configurations of amplifying loops in recent years due to its unique advantages in self-starting mode-locking and environmental stability. For instance, F9 Erbium-doped fiber laser (EDFL) based on simple mirror [7], nonlinear phase shifter [8,9], NALM [10,11], and liquid crystal variable retarders [12], F9 Ytterbium-doped fiber laser (YDFL) based on NALM [13], chirped fiber Bragg grating (CFBG) [14], wave plates incorporated with grating pairs [15], and NALM incorporated with FBG [16], F9 Thulium-doped fiber laser (TDFL) based on NALM incorporated with CFBG [17] and FLM Kharitonov and [18], and F9 HDFL based on NALM [2]. The above discussed comprehensive literature review reveals that F9 HDFLs have not yet been extensively researched earlier. We report a 12.5 MHz femtosecond pulse width F9 HDFL operating at 2090 nm wavelength based on a single 0.3 W 1950 nm forward pump and external reflector. The F9 HDFL is implemented by using three different reflectors. The proposed F9 HDFL's performance is compared across different reflectors using key laser output parameters. SA, SM, and FLM configurations yield mode-locked pulses with SEs of 35.6%, 8%, and 8.8%, pulse widths of 357.2 fs, 294 fs, and 231 fs, OSNRs of 36.4 dB, 46 dB, and 50 dB, peak powers of 13.53 kW, 6.12 kW, and 9 kW, and pulse energies of 4.83 nJ, 2 nJ, and 2.1 nJ, respectively.

Based on above discussion, the novel findings of this work are:

- Demonstration of passively mode-locked F9 HDFL operating at 2090 nm implemented with different external reflectors.
- In contrast to earlier loop-mirror based designs, this work systematically investigates different reflection methods, revealing their significant impact on pulse quality, and providing new design guidelines for the 2000 nm spectral region.
- Comparison of three different reflectors (SA, SM, and FLM) reveals FLM's superior pulse quality (231 fs pulse width, 50 dB OSNR) versus SA's energy advantage (13.53 kW peak power).
- Achievement of 12.5 MHz repetition rate femtosecond pulses enabled by the F9 cavity's nonlinearity management.

The proposed design and analysis of passively mode-locked F9 HDFL is performed using OptiSystem 21 commercial software developed by Optiwave Inc., Ontario, Optiwave Inc [19]. This paper is organized as follows: Section 2 presents the theoretical framework, Section 3 describes the proposed design implemented using OptiSystem software, Section 4 provides a comprehensive analysis of the results, and finally Section 5 concludes with key findings and implications.

2 Theoretical background

To completely understand the operating mechanism of the proposed F9 HDFL operating in mode-locking regime, it is essential to understand the main dynamics of Ho^{3+} doped in silica through spectroscopic analysis along with the working of F9 cavity.

2.1 Spectroscopic analysis of holmium

Figure 1 shows the normalized absorption and emission cross-section spectra of Ho^{3+} ions in a silica host, along with a four-level energy diagram illustrating the most commonly occurring transitions. The Ho^{3+} ions exhibit a broad absorption band extending from 1800 nm up to 2100 nm, with maximum absorption occurs at approximately 1950 nm [20,21]. In practical implementations, these ions are efficiently excited through in-band pumping at either 1950 nm or 1840 nm wavelengths, typically achieved using TDFL based pump sources. The Ho^{3+} ions residing at ground energy state $^5I_8$ are excited to the $^5I_7$ level through ground state absorption (GSA) using in-band pumping as mentioned above. The transition governing the GSA and corresponding lasing at 2000 nm is $^5I_7 \rightarrow {}^5I_8$. This GSA process and the corresponding lasing transitions are clearly indicated by red arrows at the absorption and emission spectra of Figure 1a.

2.2 Operating principle of F9 HDFL cavity

The F9 HDFL cavity is implemented utilizing three different external reflectors in this work. The mode-locking of the proposed laser is achieved through a combination of interference and nonlinear pulse shaping. The laser cavity splits into two paths at a 50:50 optical coupler where one path contains the gain medium which is HDF while the other consists of an external reflector. Pumping the HDF generates

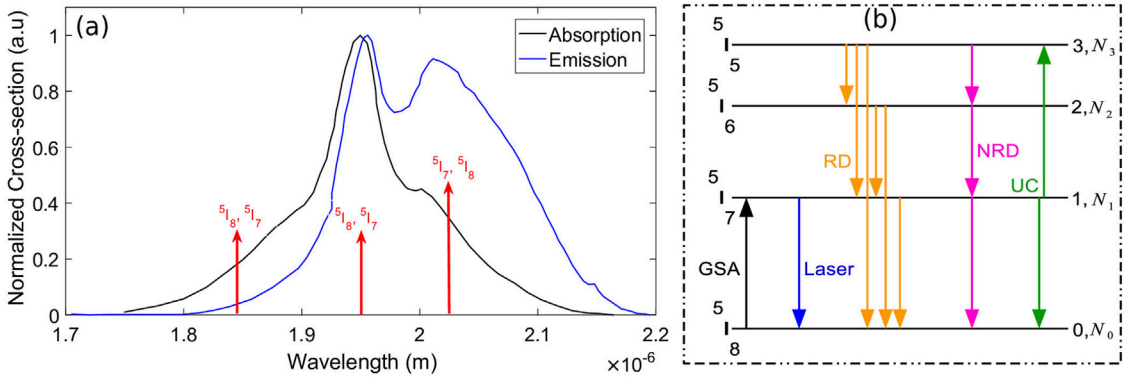

FIGURE 1
(a) Ho^{3+} absorption and emission cross-section **(b)** Energy level diagram.

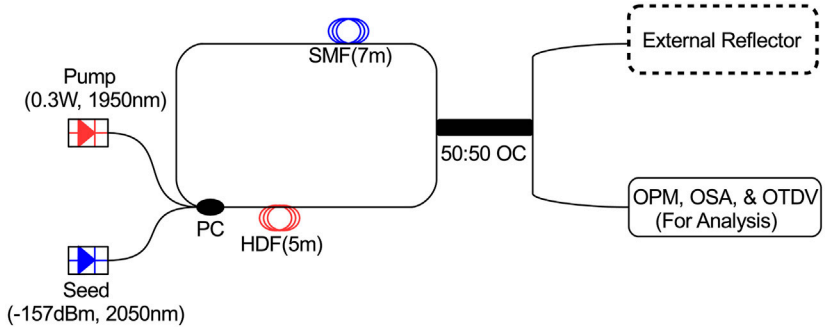

FIGURE 2
F9 HDFL block diagram, HDF: Holmium-doped fiber, SMF: Single-mode fiber, PC: Pump combiner, OC: Optical coupler, OPM: Optical power meter, OSA: Optical spectrum analyzer, OTDV: Optical time-domain visualizer.

a wideband amplified spontaneous emission (ASE) signal in the NALM loop that is combined with the seed laser for injection seeding. The ASE is allowed to propagate through the HDF repeatedly and gets amplified. When light circulates in the NALM loop, part of it travels through the HDF where intensity-dependent nonlinear effects sharpen the pulse while the rest reflects off the reflector and recombines with the main beam. This interference selectively reinforces high-intensity pulses while suppressing weaker continuous wave (CW) light, effectively working like an artificial saturable absorber. The mirror's fixed reflection ensures consistent pulse timing and its distance from the coupler fine-tunes the pulse duration, resulting into stable and self-sustaining pulses. The mode-locking threshold in a F9 HDFL is determined by the nonlinear phase accumulation in the cavity. When the nonlinear phase shift $\Delta\phi_{NL}$ exceeds $\pi/2$, the system transitions from CW to mode-locked operation. This phase shift depends on the peak power P_{peak} as [22]:

$$\Delta\phi_{NL} = 2\gamma P_{peak} L_{eff} \tag{1}$$

In Equation 1, $\gamma = n_2\omega_0/(cA_{eff})$ represents the nonlinear coefficient ($n_2 \approx 2.6\times10^{-20}$ m^2/W for silica fibers), and $L_{eff} = (1-e^{-\alpha L})/\alpha$ is the effective fiber length accounting for attenuation α at 2090 nm. The threshold condition $\Delta\phi_{NL} \geq \pi/2$ yields the critical peak power as given in Equation 2 [22].

$$P_{th} = \frac{\pi}{4\gamma L_{eff}} \tag{2}$$

For typical HDF parameters with $L_{eff} \approx 5$ m and $A_{eff} = 50$ μm^2, this threshold occurs at approximately 100.6 W peak power. The FLM's power-dependent reflectivity $R = \sin^2[(\Delta\phi_0 + \Delta\phi_{NL})/2]$ creates intensity discrimination essential for passive mode-locking, where $\Delta\phi_0$ is the static phase bias introduced by the 50:50 coupler.

Equation 3 defines the pulse evolution in HDF by modified Ginzburg–Landau equation [23].

$$\frac{\partial A}{\partial z} = \frac{g}{2}A + i\frac{\beta_2}{2}\frac{\partial^2 A}{\partial T^2} + i\gamma|A|^2A + \frac{g}{2\Omega_g^2}\frac{\partial^2 A}{\partial T^2} \tag{3}$$

accounting for gain (g), dispersion ($\beta_2 \approx -50$ ps^2/km at 2090 nm), Kerr nonlinearity, and gain bandwidth ($\Omega_g \sim 10$ nm). The quasi-three-level nature of Ho^{3+} ions introduces additional threshold considerations through the pump power requirement [23].

$$P_{pump,th} \approx \frac{h\nu_p}{\sigma_a\tau}\left(1 + \frac{\sigma_e}{\sigma_a}\right) \tag{4}$$

TABLE 1 Simulation parameters of F9 HDFL.

Sr. No	Parameter	Value
1	Pump wavelength	1950 nm
2	Pump power	300 mW
3	Seed wavelength	2050 nm
4	Seed power	−157 dBm
5	HDF length	5 m
6	Ho^{3+} concentration	15×10^{24} m^{-3}
7	HDF core radius	4 μm
8	HDF doping radius	2 μm
9	Numerical aperture	0.3 nm
10	Length of SMF	7 m
11	Attenuation	0.2 dB/km
12	Reflectivities of reflectors	99%
13	Resolution bandwidth of OSA	0.01 nm
14	Coupling ratio of OC	50%
15	Sequence length	1 bit
16	Samples per bit	1024

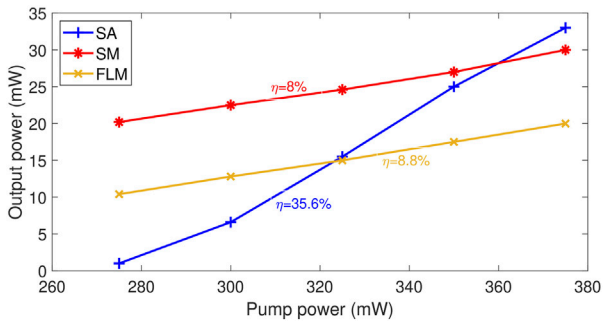

FIGURE 3
Pump power versus output power plots of F9 HDFL using three different reflectors.

In Equation 4, σ_a and σ_e are the absorption and emission cross-sections respectively, and $\tau \approx 2$ ms is the upper-state lifetime. Compared to SM or SA configurations, the FLM approach offers superior stability against environmental perturbations while maintaining lower mode-locking thresholds, as evidenced by the simulation results showing 50 dB OSNR and 231 fs pulse width in this work.

3 Proposed passively mode-locked F9 HDFL

Figure 2 illustrates the block diagram of the proposed passively mode-locked F9 HDFL. The F9 cavity consists of a NALM loop, an external reflector, a seed laser for injection seeding, and 1950 nm laser diode for pumping the gain fiber. Injection seeding is a technique which is mostly applied to pulsed lasers and optical parametric oscillators, usually with the main goal of achieving single-longitudinal mode operation alongwith reduced pulse build-up time, increases pulse energy, and reduces timing jitter in Q-switched lasers. The NALM loop consists of two short pieces of HDF and single-mode fiber (SMF) having lengths of 5 m and 7 m, respectively, a pump combiner (PC) used to combine the pump and seed laser with the HDF, and an output optical x-coupler (OC) with 50:50 splitting ratio whose power dependent reflectivity contributes in enabling the passive mode-locking. PC component in OptiSystem is basically pump-coupler for combining signals and pumps. It is bidirectional component with wavelength dependent isolation, insertion loss, and return loss. Commercially, different variants of PCs with N number of pumps and one signal input are available, denoted as $(N+1)\times 1$. PCs without a signal input are denoted as $N \times 1$. The 50:50 OC's transfer function is defined by Equation 5 [24].

$$\begin{bmatrix} E_3 \\ E_4 \end{bmatrix} = \frac{1}{\sqrt{2}} \begin{bmatrix} 1 & i \\ i & 1 \end{bmatrix} \begin{bmatrix} E_1 \\ E_2 \end{bmatrix} \tag{5}$$

where E_1 and E_2 are input optical fields while E_3 and E_4 are output optical fields. The parameters of HDF used in this work are similar to the commercial HDF (Model#iXblue IXF-HDF-PM-8–125) [25]. To achieve optimum operating conditions, the length of HDF and Ho^{3+} concentration are very similar to operating conditions described in [26]. The external reflector is connected to one of the output ports of the 50:50 OC, as shown in Figure 2. The F9 HDFL cavity is implemented using three different external reflectors including SA, SM, and FLM having 99% reflectivity in this work. The reflectivity of SA is modelled by the transfer function as given in Equation 6 [27].

$$R(t) = R_{\text{unsat}} + \frac{R_{\text{sat}} - R_{\text{unsat}}}{1 + P(t)/P_{\text{sat}}} \tag{6}$$

where R_{unsat} represents the unsaturable reflectance, R_{sat} is the saturable reflectance, P_{sat} denotes the saturation power, and $P(t)$ corresponds to the instantaneous pulse peak power. Similarly, reflectivity of SM is modelled by the transfer function given in Equation 7 [28].

$$E_{\text{out}} = E_{\text{in}} R \tag{7}$$

where R is the surface reflection coefficient. The reflectivity of FLM is modelled by the trasnfer function given in Equation 8 [24].

$$R_{\text{FLM}} = \sin^2\left(\frac{\Delta\phi}{2}\right) \tag{8}$$

where $\Delta\phi = \phi_1 - \phi_2$ is the phase difference between counter-propagating waves and ϕ_1, ϕ_2 are the phases accumulated in each direction. Different optical visualizers, such as optical power meter (OPM), optical spectrum analyzer (OSA), and optical time-domain visualizer (OTDV) are used for monitoring of the results by

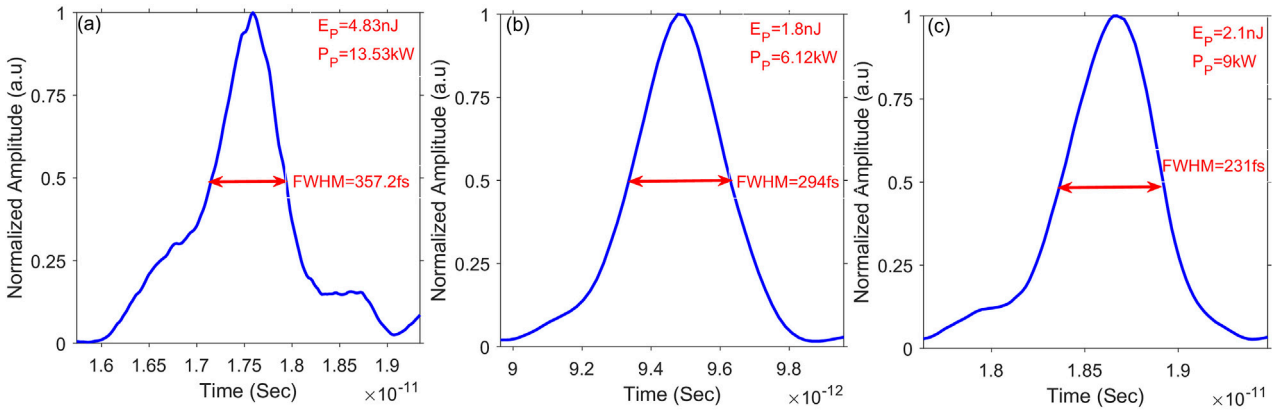

FIGURE 4
Time-domain traces of mode-locked pulses generated from F9 HDFL using different reflectors **(a)** Saturable absorber **(b)** Simple mirror **(c)** Fiber loop mirror. Cavity runs with a same repetition rate of 12.5 MHz for each reflector case.

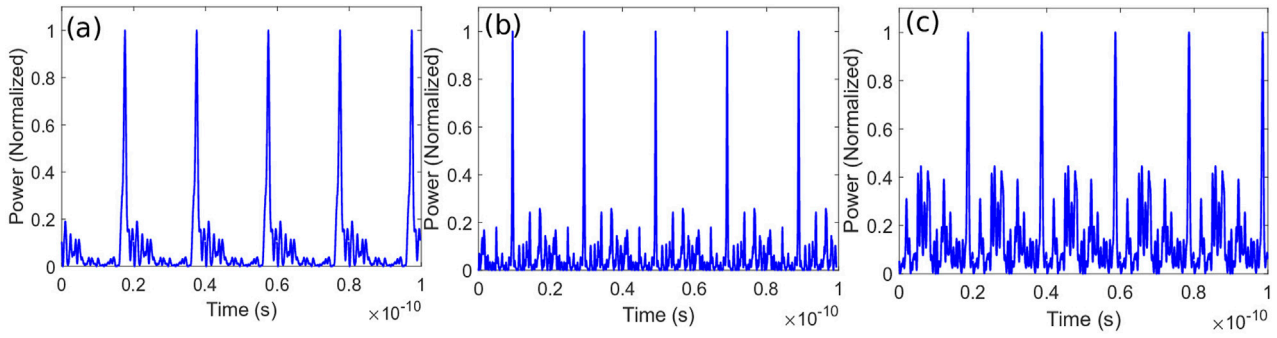

FIGURE 5
Time-domain traces of mode-locked pulse trains generated from F9 HDFL using different reflectors **(a)** Saturable absorber **(b)** Simple mirror **(c)** Fiber loop mirror. Cavity runs with a same repetition rate of 12.5 MHz for each reflector case.

connecting with second output port of 50:50 OC as shown in Figure 2. Table 1 shows the important simulation parameters used in this work.

Each of the different reflectors used in the F9 HDFL interacts and affects the lasing mechanism in a different way. The FLM based design of F9 HDFL acts like SM with different behavior which is related to suppressing half of the reflected noise into the cavity. The SM does not have such behavior as it reflects both the lasing signal and noise equally. Also, both the FLM and SM do not have interaction with the lasing power as they are passive devices, which avoids any nonlinear interaction. On the other hand, the FLM length is short, which will not cause any dispersion to the produced pulses. However, it affects the width of the produced pulses as it affects the laser cavity length. The SA based design of F9 HDFL interacts with the lasing signal power and pump power which affects the reflected signal ratio into the laser cavity. The interaction eventually affects the final pulse width of the laser. Moreover, the laser cavity is fixed for all reflector cases because the fiber length is constant. However, the percentage of the reflected signal into the cavity varies from one type to another. As described above, the SA reflection depends on the power applied on it, while the FLM reflects 3 dB less power into the loop for the ASE, while reflecting all the lasing signal. However, the SM reflects both the ASE and lasing signal fully into the cavity. As a result, the mode-locking threshold varies for each reflector.

4 Results and discussion

Figure 3 shows pump power versus output power plots of passively mode-locked F9 HDFL for three different reflectors such as SA, SM, and FLM. The relationship between output power and pump power, as shown in Figure 3 is clearly demonstrating a linear dependence. As evidenced by the plots, the measured SEs are 35.5%, 8%, and 8.8% for SA, SM, and FLM based designs of F9 HDFL, respectively. The SEs differ for each design primarily due to variations in intracavity losses and nonlinear effects introduced by the different reflectors.

Figure 4 shows the time-domain traces of mode-locked pulses measured by OTDV generated from passively mode-locked F9 HDFL using SA, SM, and FLM configurations as shown in Figure 2. It is clearly evident that the pulse widths of 357.2 fs, 294 fs, and 231 fs, peak powers (P_p) of 13.53 kW, 6.12 kW, and 9 kW, and pulse

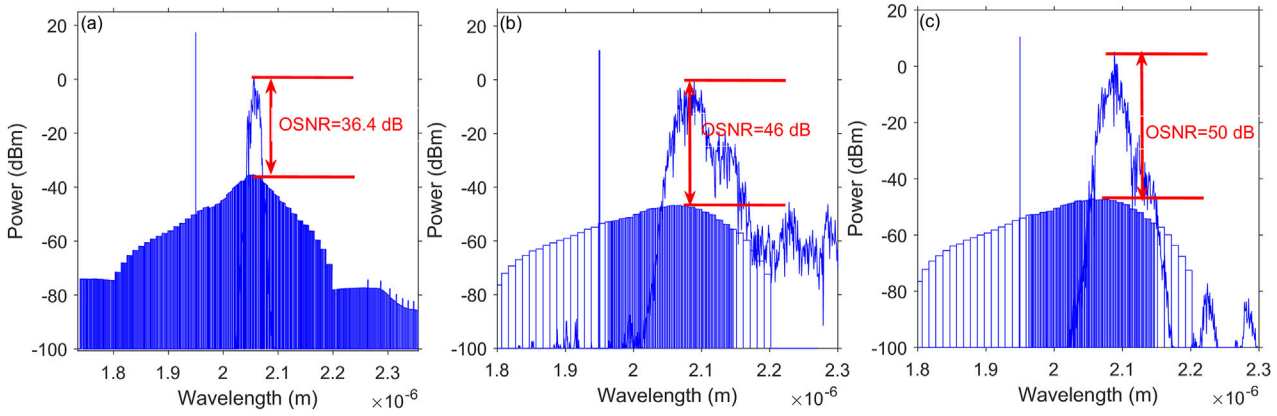

FIGURE 6
Frequency-domain plots of mode-locked pulses generated from F9 HDFL using different reflectors **(a)** Saturable absorber **(b)** Simple mirror **(c)** Fiber loop mirror. Cavity runs with a same repetition rate of 12.5 MHz for each reflector case.

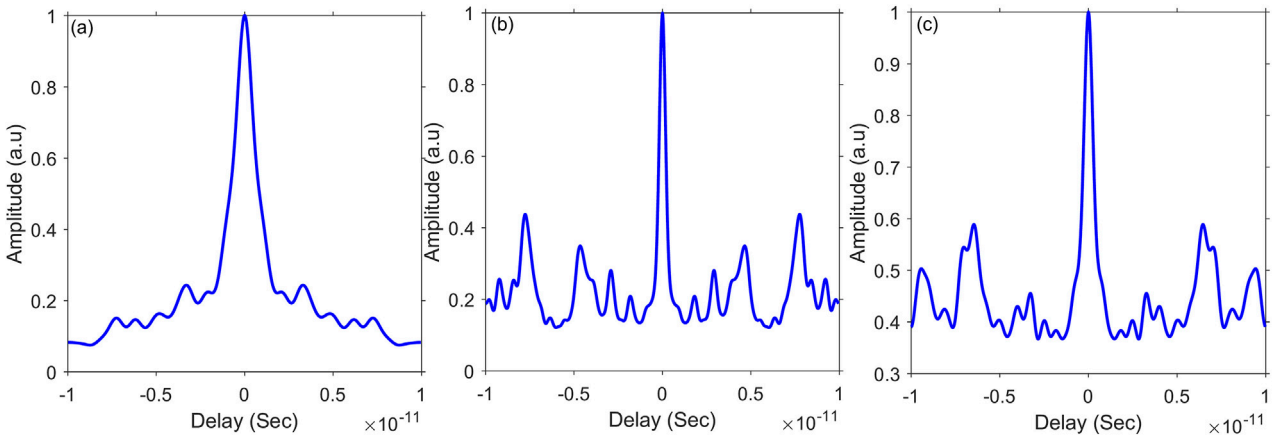

FIGURE 7
Auto-correlation traces of generated mode-locked pulses for different reflectors **(a)** Saturable absorber **(b)** Simple mirror **(c)** Fiber loop mirror. Cavity runs with a same repetition rate of 12.5 MHz for each reflector case.

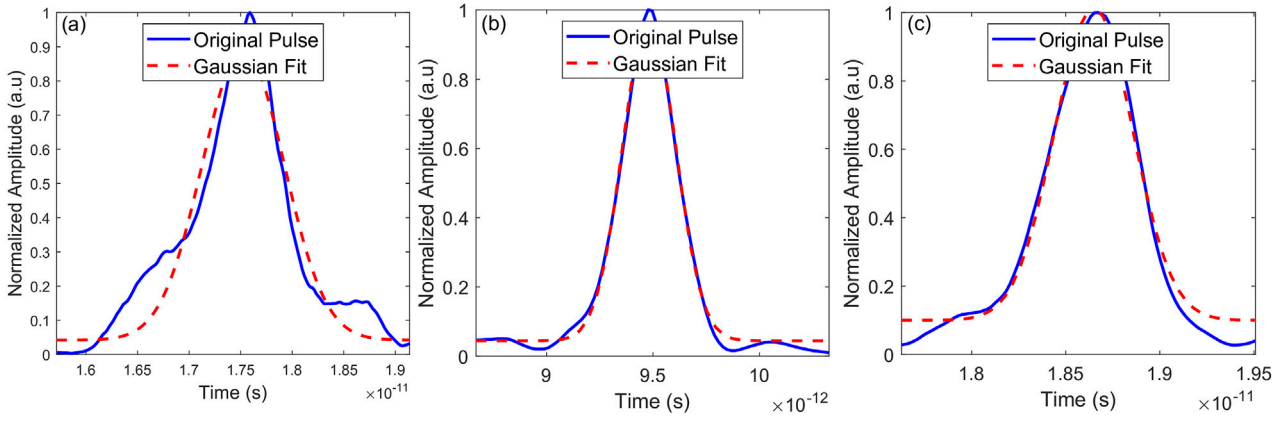

FIGURE 8
Time-domain traces of mode-locked pulses generated from F9 HDFL with Gaussian fittings using different reflectors **(a)** Saturable absorber **(b)** Simple mirror **(c)** Fiber loop mirror. Cavity runs with a same repetition rate of 12.5 MHz for each reflector case.

TABLE 2 Performance benchmarking and comparison of the proposed work with related published experimental studies.

Ref.	Cavity	Rate	SE	Energy	Pulse width	Avg. power	OSNR
Wang et al. [2]	F9, NALM	1.855 MHz	16.6%	280 nJ	-	520 mW	56 dB
Filatova et al. [30]	Ring, NPE	20.4 MHz	-	0.3 nJ	1.3 ps	6.12 mW	65 dB
Proposed	F9, NALM	12.5 MHz	35.6%	4.83 nJ	357.2 fs	60.4 mW	36.4 dB

energies (E_p) of 4.83 nJ, 2 nJ, and 2.1 nJ are obtained using SA, SM, and FLM configurations, respectively. Figure 5 shows the time domain plots of mode-locked pulse trains for SA, SM, and FLM configurations as shown in Figure 2 at wavelengths and repetition rate of 2090 nm and 12.5 MHz, respectively.

Figure 6 shows the spectral plots of mode-locked pulses measured by OSA generated from passively mode-locked F9 HDFL using SA, SM, and FLM configurations as shown in Figure 2. It is clearly evident that the OSNRs of 36.4 dB, 46 dB, and 50 dB are obtained using SA, SM, and FLM configurations, respectively. The OSNRs differ because each reflector filters noise differently. The FLM's interferometric design suppresses noise most effectively compared to the SA and SM designs. The FLM is a passive module acts as a mirror with noise filter characteristics [29]. As a result, the FLM produces better OSNR compared to the SA and SM, that do not have the noise reduction mechanisms. Moreover, the residual pump is clearly visible in spectral plots due to small conversion efficiency and length of the HDF. It doesn't absorb all the pump. However there should be enough ASE to start the lasing process to overcome the loss in the HDF. Often it has been observed that all pump power does not fully absorb in the gain fiber and residual pump power can be extracted and used for different purposes such as pumping the gain fiber in dual stage amplifier, pump recycling, SE improvement, and self-pulsing.

Figure 7 shows the auto-correlation traces of mode-locked pulses measured by OTDV generated from passively mode-locked F9 HDFL using SA, SM, and FLM configurations as shown in Figure 2. The auto-correlation traces show that the FLM produces the shortest and cleanest pulses, while the SA generates longer but more energetic pulses. The SM results in pulses with intermediate characteristics. These measurements confirm the pulse duration differences. The cleaner trace of the FLM also aligns with its higher OSNR performance.

The Gaussian fitting of the mode-locked pulses generated from the passively mode-locked F9 HDFL reveals critical insights into the temporal characteristics of each reflector design as shown in Figure 8. For the SM configuration, Figure 8b illustrates the close Gaussian fit ($R^2 > 0.98$) confirms near-transform-limited pulses with minimal chirp, though the broader FWHM of 294 fs indicates some residual dispersion effects. Similarly, Figure 8c shows the FLM's excellent Gaussian match ($R^2 > 0.99$) validates its ability to generate near-ideal, symmetric pulses of 231 fs pulse width, consistent with its superior OSNR performance, suggesting optimal nonlinear phase compensation. Notably in SA based design, Figure 8a shows slight deviation from Gaussian shape at pulse wings hints at minor uncompensated nonlinearities, explaining its intermediate performance. These fits quantitatively demonstrate how SA prioritizes energy retention while FLM optimizes temporal purity which is the key considerations for applications demanding either high peak power or precision pulse shaping. The Gaussian analysis further supports the cavity's ability to sustain stable soliton-like pulses across all configurations.

For performance benchmarking, we have compared the main results of the proposed F9 HDFL with related published experimental works in Table 2.

5 Conclusion

This work demonstrated femtosecond passively mode-locked Holmium-doped fiber laser operating at 2090 nm based upon a Figure-9 cavity which was implemented with three distinct reflectors including saturable absorber, simple mirror, and fiber loop mirror. A comparative analysis of the laser's performance based on metrics including slope efficiency, pulse duration, optical signal to noise ratio, peak power, and pulse energy was conducted for each reflector configuration. The figure-9 Holmium-doped fiber laser performed differently with each reflector. The saturable absorber based design gave the highest slope efficiency and peak power of 35.6% and 13.53 kW, respectively with pulse width of 357 fs. The fiber loop mirror configuration generated the mode-locked pulses having pulse width of 231 fs and optical signal to noise ratio of 50 dB OSNR with 9 kW peak power. The performance of simple mirror based design was in between. The figure-9 cavity's versatility enables tailored operation across ultrafast and high-energy regimes, advancing 2000 nm laser technology for optical wireless communication and beyond.

Data availability statement

The original contributions presented in the study are included in the article/supplementary material, further inquiries can be directed to the corresponding author.

Author contributions

JM: Conceptualization, Investigation, Methodology, Software, Validation, Visualization, Writing – original draft, Writing – review and editing. AAt: Conceptualization, Software, Writing – original draft, Writing – review and editing. SB: Methodology, Visualization, Writing – original draft, Writing – review and editing. BK: Formal Analysis, Methodology, Validation, Writing – original draft, Writing – review and editing. IA: Project administration, Resources,

Validation, Writing – original draft, Writing – review and editing. AAl: Funding acquisition, Resources, Validation, Writing – original draft, Writing – review and editing.

Funding

The author(s) declared that financial support was received for this work and/or its publication. This work was supported by King Saud University, Riyadh, Saudi Arabia, through ongoing research funding program (ORF-2026-184).

Conflict of interest

Author AAt was employed by Optiwave Systems Inc.

The remaining author(s) declared that this work was conducted in the absence of any commercial or financial relationships that could be construed as a potential conflict of interest.

Generative AI statement

The author(s) declared that generative AI was not used in the creation of this manuscript.

Any alternative text (alt text) provided alongside figures in this article has been generated by Frontiers with the support of artificial intelligence and reasonable efforts have been made to ensure accuracy, including review by the authors wherever possible. If you identify any issues, please contact us.

Publisher's note

References

1. Wang C, Liu J, Zhang Z. Transmission characteristics of femtosecond laser pulses in a polymer waveguide. *Opt Express* (2022) 30:31396–406. doi:10.1364/OE.467884

2. Wang J, Han J, He J, Liao C, Wang Y. High-energy mode-locked holmium-doped fiber laser operating in noise-like pulse regime. *Opt Lett* (2019) 44:4491–4. doi:10.1364/OL.44.004491

3. Tu L, Tang Z, Li K, Wang J, Lin H, Zhang W, et al. All-polarization-maintaining mode-locked holmium-doped fiber laser based upon nonlinear polarization evolution. *Infrared Phys and Technology* (2024) 136:105054. doi:10.1016/j.infrared.2023.105054

4. Mirza J, Atieh A, AlQahtani S, Ghafoor S. A high power and repetition rate wavelength tunable actively mode-locked holmium-doped fiber laser for bidirectional transmission between two haps. *Opt Quan Electronics* (2023) 55:1248. doi:10.1007/s11082-023-05471-8

5. Kanwal B, Atieh A, Ghafoor S, Sajid M, Mirza J. Design and performance of a repetition rate controllable and wavelength tunable l+ u-band actively mode-locked erbium fiber laser. *J Opt Soc America B* (2023) 40:1644–51. doi:10.1364/josab.489410

6. Yao G, Zhao Z, Liu Z, Gao X, Cong Z. High repetition rate actively mode-locked er: fiber laser with tunable pulse duration. *Chin Optics Letters* (2022) 20:071402. doi:10.3788/col202220.071402

7. Deng Q, Yin K, Zhang J, Zheng X, Jiang T. A 200 mhz compact environmentally-stable mode-locked figure-9 fiber laser. *IEEE Photon J* (2021) 13:1–5. doi:10.1109/jphot.2021.3095159

8. Duan D, Wang J, Wu Y, Ma J, Mao Q. Approach to high pulse energy emission of the self-starting mode-locked figure-9 fiber laser. *Opt Express* (2020) 28:33603–13. doi:10.1364/OE.409406

9. Chen W-B, Li T-J, Tong L-Y, Yang K, Liu M, Luo A-P, et al. Assisting the mode-locking of a figure-9 fiber laser by thermal nonlinearity of graphene-decorated microfiber. *Opt Express* (2023) 31:2902–10. doi:10.1364/OE.476673

10. Xiong S, Luo D, Liu Y, Wang W, Deng Z, Tang Z, et al. Investigation of stable pulse mode-locking regimes in a nalm figure-9 er-doped fiber laser. *Opt Express* (2022) 31:514–27. doi:10.1364/oe.476630

11. Pan Y, Lu Q, Ma T, Zhang D, Pan H, Liang L. All-polarization-maintaining figure-9 erbium-doped mode-locked fiber laser based on<? tex\break?> a bidirectionally pumped weak asymmetric nalm. *Appl Opt* (2024) 63:8034–43. doi:10.1364/ao.539186

12. Lu Q, Ma X, Zhang F, Wu Q, Liu H. Figure-9 mode-locked fiber laser using liquid crystal variable retarders. *Opt Express* (2025) 33:5012–20. doi:10.1364/OE.545780

13. Guo K, Li C, Ren B, Wang T, Wu J, Luo Z, et al. Highly stable q-switched and mode-locked pulse generation from an all-pm figure-9 fiber laser. *Opt Express* (2022) 30:35636–46. doi:10.1364/OE.470739

14. Tang Z, Zhang J, Luo D, Xie G, Pan J, Wang Z, et al. Compact 980-nm all-polarization-maintaining dispersion-managed figure-9 yb-doped fiber laser. *J Lightwave Technology* (2025) 43:7364–9. doi:10.1109/jlt.2025.3570106

15. Ma J, Ma M, Liu H, Shum PP. Low-noise 2-ghz figure-9 fiber laser based<? pag\break?> on passive harmonic mode-locking. *Opt Lett* (2024) 49:6401–4. doi:10.1364/OL.538386

16. Cao X, Cheng Z, Xiong Y, Li X, Ye Q, Guo Z, et al. Generating narrow bandwidth pulses in an all-fiber figure-9 mode-locked fiber laser. *IEEE J Quan Electronics* (2025) 61:1–5. doi:10.1109/jqe.2025.3541951

17. Ren B, Li C, Wang T, Guo K, Zhou P. All-polarization-maintaining figure-9 mode-locked tm-doped fiber laser with amplitude noise and timing jitter suppression. *J Lightwave Technology* (2022) 41:733–8. doi:10.1109/jlt.2022.3219984

18. Kharitonov S, Brès C-S. All-fiber dissipative soliton resonance mode-locked figure-9 thulium-doped fiber laser. In: *The European conference on lasers and electro-optics*. Munich, Germany: Optica (2017).

19. Optiwave Inc. Optisystem overview (2023). Available online at: https://optiwave.com/optisystem-overview/(Accessed on January 3, 2026).

20. Tench RE, Walasik W, Delavaux J-M. Novel highly efficient in-band pump wavelengths for medium slope efficiency holmium-doped fiber amplifiers. *J Lightwave Technology* (2021) 39:3546–52. doi:10.1109/jlt.2021.3067600

21. Mirza J, Atieh A, Kanwal B, Ghafoor S. Novel pumping scheme of holmium doped fiber amplifiers operating around 2μm using 1.48 μm lasers exploiting cascaded fiber lasers. *Optik* (2022) 262:169238. doi:10.1016/j.ijleo.2022.169238

22. Duling IN. All-fiber ring soliton laser mode locked with a nonlinear mirror. *Opt Letters* (1991) 16:539–41. doi:10.1364/ol.16.000539

23. Jackson SD. Towards high-power mid-infrared emission from a fibre laser. *Nat Photonics* (2012) 6:423–31. doi:10.1038/nphoton.2012.149

24. Agrawal GP. *Fiber-optic communication systems*. John Wiley and Sons (2012).

25. Mirza J, Ghafoor S, Almogren A, Salaria UA, Kanwal B, Aziz I, et al. Pair induced quenching in high concentration holmium-doped fiber amplifiers. *Physica Scripta* (2024) 99:055513. doi:10.1088/1402-4896/ad36f5

26. Filatova SA, Kamynin VA, Arutyunyan NR, Pozharov AS, Trikshev AI, Zhluktova IV, et al. Hybrid mode locking of an all-fiber holmium laser. *J Opt Soc America B* (2018) 35:3122–5. doi:10.1364/josab.35.003122

27. Haus HA. Theory of mode locking with a fast saturable absorber. *J Appl Phys* (1975) 46:3049–58. doi:10.1063/1.321997

28. Vorburger TV, Silver R, Brodmann R, Brodmann B, Seewig J. Light scattering methods. In: *Optical measurement of surface topography*. Springer (2011). p. 287–318.

29. Atieh A. Noise figure reduction in erbium-doped fiber amplifiers using loop mirror filter. *Fiber and Integrated Opt* (2001) 20:465–70. doi:10.1080/014680301750413421

30. Filatova S, Kamynin V, Korobko D, Fotiadi A, Lobanov A, Zverev A, et al. Experimental and numerical study of different mode-locking techniques in holmium fiber laser with a ring cavity. *Opt Express* (2024) 32:22233–48. doi:10.1364/OE.523902